




ORIGINAL ARTICLE

Using quantitative magnetic resonance imaging to track cerebral alterations in multiple sclerosis brain: A longitudinal study

Nora Vandeleene¹  | Camille Guillemin^{1,2} | Solène Dauby^{1,3} | Florence Requier^{1,2} |
Maëlle Charonitis^{1,2} | Daphne Chylinski^{1,2} | Evelyne Balteau¹ | Pierre Maquet^{1,3} |
Emilie Lommers^{1,3}  | Christophe Phillips^{1,4} 

¹GIGA CRC In Vivo Imaging, University of Liège, Liège, Belgium

²Psychology and Cognitive Neuroscience Research Unit, University of Liège, Liège, Belgium

³Clinical Neuroimmunology Unit, Neurology Department, CHU Liège, Liège, Belgium

⁴GIGA In Silico Medicine, University of Liège, Liège, Belgium

Correspondence

Christophe Phillips, GIGA CRC In Vivo Imaging, University of Liège, Liège, Belgium.
Email: c.phillips@uliege.be

Funding information

Fonds pour la Formation à la Recherche dans l'Industrie et dans l'Agriculture (FRIA), Grant/Award Number: FC 031945; Fonds de la Recherche Scientifique-FNRS (F.R.S.-FNRS) Belgium

Abstract

Introduction: Quantitative MRI quantifies tissue microstructural properties and supports the characterization of cerebral tissue damages. With an MPM protocol, 4 parameter maps are constructed: MTsat, PD, R1 and R2*, reflecting tissue physical properties associated with iron and myelin contents. Thus, qMRI is a good candidate for in vivo monitoring of cerebral damage and repair mechanisms related to MS. Here, we used qMRI to investigate the longitudinal microstructural changes in MS brain.

Methods: Seventeen MS patients (age 25–65, 11 RRMS) were scanned on a 3T MRI, in two sessions separated with a median of 30 months, and the parameters evolution was evaluated within several tissue classes: NAWM, NACGM and NADGM, as well as focal WM lesions. An individual annual rate of change for each qMRI parameter was computed, and its correlation to clinical status was evaluated. For WM plaques, three areas were defined, and a GLMM tested the effect of area, time points, and their interaction on each median qMRI parameter value.

Results: Patients with a better clinical evolution, that is, clinically stable or improving state, showed positive annual rate of change in MTsat and R2* within NAWM and NACGM, suggesting repair mechanisms in terms of increased myelin content and/or axonal density as well as edema/inflammation resorption. When examining WM lesions, qMRI parameters within surrounding NAWM showed microstructural modifications, even before any focal lesion is visible on conventional FLAIR MRI.

Conclusion: The results illustrate the benefit of multiple qMRI data in monitoring subtle changes within normal appearing brain tissues and plaque dynamics in relation with tissue repair or disease progression.

Emilie Lommers and Christophe Phillips equally contributed to the work.

This is an open access article under the terms of the [Creative Commons Attribution](https://creativecommons.org/licenses/by/4.0/) License, which permits use, distribution and reproduction in any medium, provided the original work is properly cited.

© 2023 The Authors. *Brain and Behavior* published by Wiley Periodicals LLC.

KEYWORDS

longitudinal analysis, multiple sclerosis, quantitative MRI, relaxometry

1 | INTRODUCTION

Multiple sclerosis (MS) is a chronic autoimmune disease of the central nervous system (CNS). Plaques are the pathological hallmark of MS. They are spread in acute, focal, disseminated, and recurrent way throughout the CNS and harbor variable degrees of inflammation, demyelination, gliosis, and axonal injury (Lassmann, 2013; Trapp et al., 1998). Plaques are not restricted to the white matter (WM) but are also present in the cortex and deep gray matter (GM) (Haider et al., 2016; Kutzelnigg et al., 2005; Popescu et al., 2012).

Over and above focal WM lesions, an early, diffuse, and chronic inflammation within the normal appearing white matter (NAWM) and gray matter (NAGM) is ultimately responsible for diffuse neuroaxonal loss and neurodegeneration, which is deemed responsible for a progressive accumulation of disability (Frischer et al., 2009; Haider et al., 2016; Kutzelnigg et al., 2005).

By contrast, effective repair mechanisms can occur within focal lesions but probably also in normal appearing brain tissue (NABT) (Brown et al., 2014). However, our understanding of these complex processes is still fragmentary. The difficulty of acquiring histopathological data on MS patients at various stages of the disease makes it challenging to describe the time course of injury and potential repair mechanisms in MS. Consequently, there is a need for new imaging techniques to improve the in vivo monitoring of brain damages formation, progression and repair in MS (Wang et al., 2019).

Conventional MRI (cMRI) readily depicts focal WM lesions on T2/FLAIR sequences and is able to distinguish between acute and allegedly chronic lesions. T2-hyperintensities in cMRI constitute the keystone of McDonald diagnostic criteria (Thompson et al., 2018) and also make an important contribution to the monitoring of WM lesion burden. Unfortunately, cMRI sequences do not sensitively detect cortical lesions and diffuse changes in NABT, due to a rather low sensitivity of cMR imaging for cortical lesions, mixed contrast weight, and an overall limited histopathological specificity within cerebral tissues. Quantitative MRI (qMRI) potentially overcomes these limitations by quantifying physical microstructural properties of cerebral tissue in standardized units. qMRI is more sensitive but also more specific to microstructural properties of CNS tissues. Magnetization transfer ratio (MTR) was regularly linked to cerebral macromolecular content detected by a greater percentage loss of magnetization in voxels with a higher myelin content and axons density (Callaghan et al., 2015; Schmierer et al., 2004; Tabelo et al., 2019). Postmortem studies comparing the relative contribution of these two factors indicate that myelin has a stronger and more direct influence on MTR than the axonal density, which is considered as a T1-dependent effect. Tissue water content (inflammation, edema, etc.), another T1-dependent effect, also accounts for MTR variability (Mottershead et al., 2003;

Schmierer et al., 2004; Van Waesberghe et al., 1999). However, the MT saturation (MTsat) map offers a measure which, unlike MTR, is minimally affected by longitudinal relaxation and B1 mapping inhomogeneities (Lema et al., 2017), increasing its sensitivity to myelin content. Moreover, the brain contrast to noise ratio is larger for the MTsat map than for MTR, thus improving brain tissue segmentation in healthy subjects (Helms et al., 2010; Schmierer et al., 2004). $R2^*$ was usually linked to iron and myelin contents, as paramagnetic iron and diamagnetic myelin generate microscopic field gradients in the CNS, thus shortening $T2^*$ and increasing $R2^*$ ($1/T2^*$). Orientation and density of myelin fibers are also a determining factor of $R2^*$ values (Bagnato et al., 2018; Hametner et al., 2018; Stüber et al., 2014). Iron is probably a key factor in MS monitoring as it was shown that aberrant iron metabolism occurs in the course of the disease (Stankiewicz & Neema et al., 2014). Particularly increased iron concentration within chronic active lesions (i.e., iron rim lesion) or deep gray matter structures was observed (Stankiewicz & Neema, 2014). Regarding the longitudinal relaxation rate $R1$ ($1/T1$), its three major determinants in the CNS are tissue myelination and associated axons, iron, and extracellular water contents (Granziera et al., 2021; Kolb et al., 2021; Stüber et al., 2014). Finally, proton density (PD) mostly reflects the free water content of the brain (Edwards et al., 2018).

A number of cross-sectional studies using a combination of MT, $R1$, $R2^*$, or PD parameters, comparing MS patients to healthy controls, reported significant changes in the microstructure of NABT, such as a decrease in MT, $R1$, and $R2^*$ and an increase in PD in patients (Andica et al., 2019; Bonnier et al., 2014; Engström et al., 2014; Gracien et al., 2016; Lommers et al., 2019; Lommers et al., 2021; Neema et al., 2007; Reitz et al., 2017; Stevenson et al., 2000). Few studies address the longitudinal variations in qMRI. $R2^*$ (Elkady et al., 2018; Elkady et al., 2019; Khalil et al., 2015), PD, and $T1$ were reported to increase in the basal ganglia over a period of a year (Gracien et al., 2017), whereas a decrease in MTR in NAWM was reported over 1 (Laule et al., 2003) or 2 years (Hayton et al., 2012).

Regarding focal WM plaques, qMRI emerges as an appealing biomarker to describe the dynamic processes of demyelination and remyelination. For instance, MTR was shown to sharply decrease within gadolinium enhancing lesions before recovering during the subsequent months (Douset et al., 1998; Elskamp et al., 2010; Levesque et al., 2010), and within NAWM days to weeks before the formation of a new active lesion (Fazekas et al., 2002; Filippi et al., 1998).

Because each qMRI parameter is differently sensitive to histologically measured iron and myelin contents, this approach might become a fundamental tool for longitudinal in vivo monitoring of MS lesions and NABT evolution at the tissue microstructural level.

In this longitudinal study, we investigate the evolution of four simultaneously acquired qMRI parameters (MTsat, PD, $R1$, $R2^*$) within

NABT and WM lesions of 17 MS patients—relapsing remitting (RRMS) and progressive MS (PMS)—who were scanned two times with at least a 1-year interval, following the same multiparameter mapping (MPM) protocol at 3 Tesla (Draganski et al., 2011; Tabelo, 2019).

We assessed the time course of parameter values in several tissue classes: normal appearing white matter (NAWM), normal appearing cortical and deep GM (NACGM and NADGM) as well as focal WM lesions. In addition, we related longitudinal qMRI changes within NABT to clinical course.

2 | MATERIALS AND METHODS

2.1 | Population

Seventeen patients, recruited at the specialized MS outpatient clinic of the CHU Liège, Belgium, with a diagnosis of MS according to the McDonald criteria 2010 (Polman et al., 2011), were gathered from two studies: 10 of them were part of the work reported by Lommers et al. (2019) and the other 7 were recruited from another MS study taking place at the GIGA Cyclotron Research Centre—In Vivo Imaging (Liège, Belgium) (Guillemin et al., 2022). For the first study (10 subjects), the inclusion criteria were (1) age between 18 and 65 years; (2) Expanded Disability Status Scale (EDSS) inferior or equal to 6.5; (3) absence of relapse within the previous 4 weeks; (4) absence of IVMP administration for at least 6 months prior to the study. Both RRMS and PMS patients were recruited. The second study (7 subjects) differs a bit as it comprises only RRMS patients, and the inclusion criteria were (1) age between 18 and 45, (2) EDSS between 0 and 4, (3) absence of relapse for at least 6 months prior to the study, (4) disease duration was below or equal to 5 years, (5) absence of IVMP administration for at least 6 months prior to the study. For both studies, compatibility with MRI and absence of other neurological/psychiatric diseases were required. These studies were approved by the local ethics committee (approval numbers B707201213806 and B707201835630, respectively). All patients were followed up and scanned twice on the same 3T MRI scanner, every 1 to 3 years. For each of the 17 MS patients, data from two MRI sessions were available, at T0 and T1. This cohort included 11 RRMS and 6 (primary and secondary) PMS patients. Thirteen were receiving disease-modifying treatments (DMTs). The patients' median age was 36 years (range: 25–65) and the median time interval between two scans was 30 months (range: 14–61). Demographic data appears in Table 1. Extended individual information appears in [Supplementary data](#).

2.2 | MR image acquisition

MRI data were acquired on a 3T whole-body MRI scanner (Magnetom Prisma, Siemens Medical Solutions, Erlangen, Germany). The whole-brain MRI acquisitions included a multiparameter mapping protocol (MPM), from which one can simultaneously estimate (semi)quantitative maps of magnetization transfer saturation (MTsat),

proton density (PD), longitudinal relaxation (R1), and effective transverse relaxation (R2*). This protocol arising from an international collaborative effort (Draganski et al., 2011; Tabelo, 2019) has already been used to study brain microstructure in various conditions including normal aging (Carey et al., 2018; Draganski et al., 2011; Thompson et al., 2018), brain tumor (Reuter et al., 2020), Parkinson's disease (Depierreux et al., 2021; Klein et al., 2018; Nürnberger et al., 2017), as well as MS. It consists of three colocalized 3D multiecho fast low angle shot (FLASH) acquisitions at 1 mm³ resolution and two additional calibration sequences to correct for inhomogeneities in the RF transmit field (Lutti et al., 2010; Lutti et al., 2012). The FLASH datasets were acquired with predominantly PD, T1 and MT weighting, referred to in the following as PDw, T1w, and MTw, at multiple echo times. All three had high bandwidth to minimize off-resonance and chemical shift artifacts. Volumes were acquired in 176 sagittal slices using a 256 × 224 voxel matrix. GRAPPA parallel imaging was combined with partial Fourier acquisition to speed up acquisition time to approximately 20 min. An additional FLAIR sequence was recorded with spatial resolution 1 mm³ and TR/TE/TI = 5000 ms/516 ms/1800 ms. Extra B1 field mapping images (transmit B1+ and receive B1- fields) were also acquired to reduce spatial inhomogeneities related to B1 effect. This was essential for proper quantification of T1 (or R1 = 1/T1) in particular. Finally, B0 field mapping images, corresponding to both magnitude images and presubtracted phase image, were acquired for image distortions corrections. A summary of the acquisition parameters appears in [Supplementary data](#).

Note that these MR sequences at 3 Tesla are not sensitive to cortical lesion as described in Filippi et al. (2013) and Hulst and Geurts (2011) although a few lesions at the corticosubcortical border were detected. Quantification of cortical parameters is thus confounded by voxels potentially located within cortical lesions.

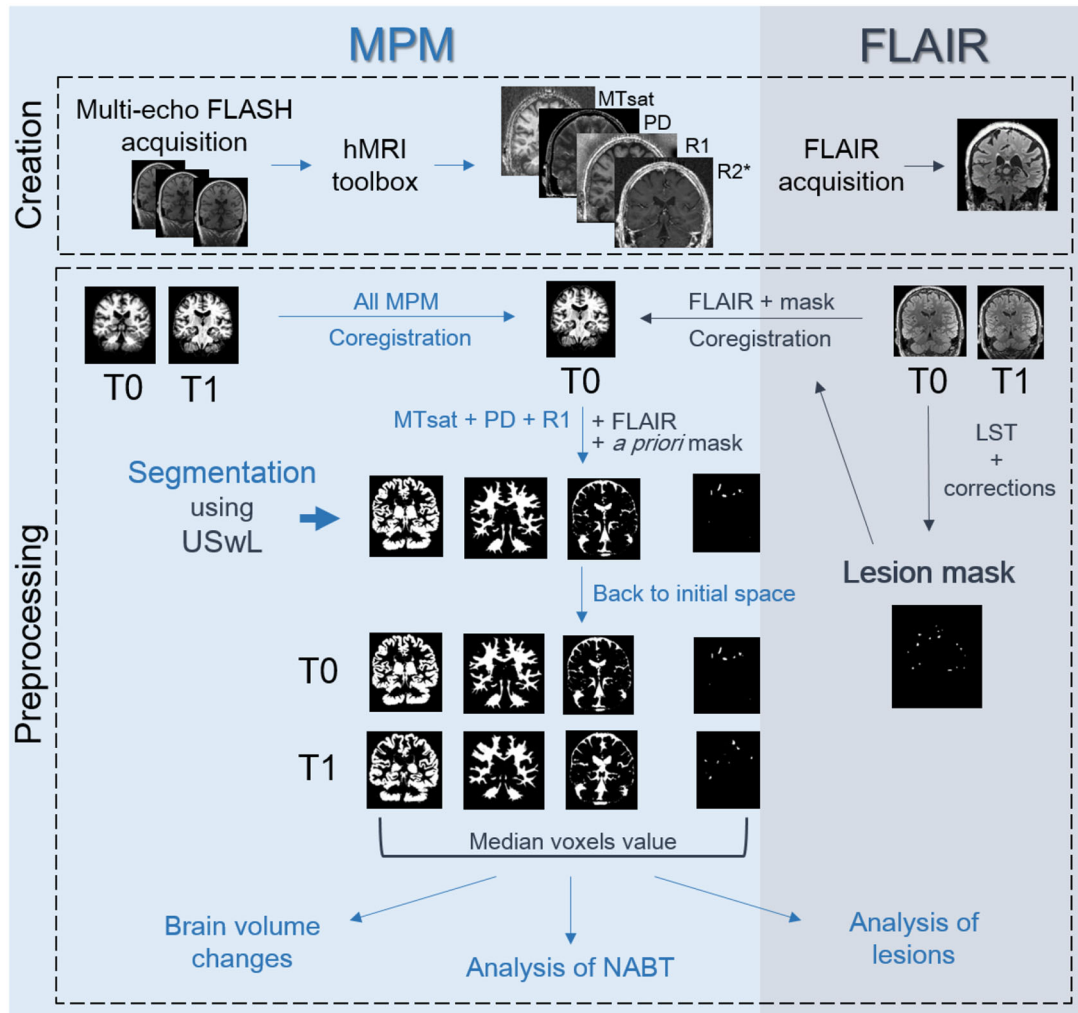
2.3 | MR image processing

All data processing was performed in Matlab (The MathWorks Inc., Natick, MA, USA) using SPM12 (www.fil.ion.ucl.ac.uk/spm) and three additional dedicated SPM extensions: the Lesion Segmentation Tool (LST) version 1.2.3 (www.statisticalmodelling.de/lst.html) (Schmidt et al., 2012), the “quantitative MRI and in vivo histology using MRI” toolbox (hMRI, <http://hmri.info>) (Tabelo, 2019), and “US-with-Lesion” tool (USwL, <https://github.com/CyclotronResearchCentre/USwLesion>).

Quantitative maps—MTsat, PD, R1 and R2*—were estimated using the hMRI toolbox. T1w, PDw, and MTw images acquired at multiple echo times (TE) were extrapolated to TE = 0 to increase signal-to-noise ratio and remove the otherwise remaining R2* bias (Lommers et al., 2019; Tabelo, 2019; Weiskopf et al., 2014). The TE = 0 extrapolated MTw, PDw, and T1w images were used to calculate MT saturation, R1, and apparent signal amplitude A* maps. PD map was derived from A* map, which is proportional to proton density. All quantitative maps were corrected for inhomogeneities from local RF transmit field (B1+), and R1 quantitative maps were further corrected for imperfect RF

TABLE 1 Demographic data of the study sample

	All patients (n = 17)	
Age, year, median (range)	36 (25–65)	
Sex, F/M	7/10	
MS phenotype (RRMS/MS)	11/6	
Baseline disease duration, year, median (range)	3.4 (0.3–28)	
Baseline EDSS, median (range)	2.5 (1–6.5)	
Baseline number of relapses, median (range)	RRMS: 2 (1–5)	PMS: N/A
Disease-modifying treatment	RRMS: first line, n: 5 second line, n: 6	PMS: ocrelizumab, n: 2 none, n: 4

**FIGURE 1** Chart flow of data creation and processing (see text). MPM maps were created with the hMRI toolbox, and FLAIR images were directly acquired for both sessions (T0 and T1). A preliminary mask was constructed based on T0 FLAIR. All images (MPM and FLAIR, T0 and T1) were coregistered to the MPM T0 space. Segmentation using USwL allowed to isolate the different tissue classes.

spoiling using the strategy of Preibisch and Deichmann (2009). The receive bias field map (B1-) was used to correct PD maps for instrumental biases. The R2* map was estimated from all three multiecho series (MTw, PDw, and R1w) using the ESTATICS model (Weiskopf et al., 2014).

After generating quantitative maps using the hMRI toolbox for all sessions, spatial preprocessing involved the following steps (Figure 1): within-patient registration brought the two serial MR data sets into the individual T0 space, using the longitudinal registration tool from SPM (Ashburner & Ridgway, 2013). For each individual patient, a preliminary

WM lesion mask was generated based on FLAIR and T1w images by the lesion growth algorithm implemented in the LST toolbox (Schmidt et al., 2012), followed by manual corrections by an MS expert (EL) to remove aberrant/artifactual lesion detections (Lommers et al., 2019). The images were then segmented using the USwL toolbox, which consists of an extended version of the traditional Unified Segmentation (US) algorithm (Ashburner & Friston, 2005) and includes an additional tissue class representing the WM lesion(s). The US-with-lesion method internally generates a subject-specific extended set of tissue probability maps (TPM) (Lorio et al., 2016): an extra tissue class, based on the smoothed preliminary lesion mask warped into template space (using cost function masking during normalization; Andersen et al., 2010), is added to account for the lesion, and the original white matter prior map is updated accordingly (Moon et al., 2002). The gray matter TPM was not updated due to a very low number of lesions present in the cortical ribbon. Multichannel segmentation was conducted, using MTsat, PD, R1, and FLAIR images. This pipeline did not use the PD-, T1-, and MT-weighted images acquired for the MPM maps construction, but the parametric maps themselves instead. In this way, voxels do not depict MR intensities but rather physical quantitative parameters. The method generated the segmented tissue classes (a posteriori tissue, including lesion, probability maps), as well as spatial warping into standard template space. The preliminary lesion mask was used as input for the first session data (at T0) then the a posteriori lesion map generated at this initial step served as prior to the subsequent session (at T1).

Segmentation teased out the different tissue classes of interest: NAWM, NACGM, and NADGM, as well as WM lesions. To analyze the microstructure within those tissue classes, a posteriori tissue maps were binarized and tissue-specific independent masks were constructed: each voxel is assigned to one single tissue class with the highest probability for that voxel (provided that this probability was above 0.2). The lesion binary mask was further cleaned for lesions $< 10 \text{ mm}^3$ which likely resulted from segmentation errors. Finally, binarized tissue class masks were in turn applied on the MPM maps to extract voxel values inside them.

2.4 | Brain volume change

Volumetric changes were investigated using the USwL a posteriori tissue probability maps. The following measures of brain volume were computed for each session of each participant: (1) total intracranial volume (TIV) = volume (NAWM + GM + CSF + lesions), (2) brain parenchymal fraction (BPF) = volume (NAWM + GM + lesions)/TIV, (3) gray matter fraction (GMF) = volume (GM)/TIV, and (4) lesion fraction (LF) = volume (lesion)/TIV. The percentage of change between both scanning sessions was evaluated for each volumetric measurement, then annualized changes were computed by dividing these measures by scan intervals (in years). Results were directly analyzed with a *t*-test (testing if significantly different from 0 at $p < .05$), but also in the same way as the normal appearing tissues MR parameters in relation to the patients' clinical status (see next section).

2.5 | Analysis of normal appearing tissues

The median value of quantitative MRI parameters was extracted from the three normal appearing tissues (NAWM, NACGM and NADGM), and an individual annual rate of change (ARoC) was computed for each parameter in each tissue class, based on the initial and final values and accounting for the time interval (in years) between scans. This rate of change in qMRI parameters served as dependent variable in a general linear model testing the effect of clinical status:

$$Y = \beta_0 + \beta_1 X_{status} + \epsilon,$$

where Y is the ARoC for a qMRI parameter and tissue class, β 's are the regression parameters corresponding to the associated regressor (with β_0 the intercept), and ϵ the residuals. X_{status} is a binary categorical variable representing the patient's disease activity status: a status score of 1 was assigned to patients stable or improving from T0 to T1.

This patient status X_{status} was derived from one score of disease activity: NEDA-3 (No Evidence of Disease Activity; Pandit, 2019), a composite of three related measures of disease activity. A score of 0 was assigned in the presence of new clinical relapses (only concerning RRMS patients) and/or MRI activity (new or enlarged lesions visible on FLAIR T2 or Gadolinium-enhanced images) and/or sustained disability progression over 6 months based on Expanded Disability Status Scale (EDSS). For both RRMS and PMS patients, disability progression was defined as a 1.0-point increase if the EDSS score was ≤ 4.0 at baseline and as a 0.5-point increase if the baseline EDSS score was > 4.0 . The threshold of 4.0 was proposed in this study because it is considered as a milestone regarding ambulatory performance.

NEDA-3 and was evaluated at mid- and end-scanning interval, and a final status score of 0 was given only to patients for which disease activity or progression was noted in both cases, indicating a clear progression of the disease over the whole interscan interval.

The influence of several clinical measurements such as 25 FWT, 9HPT, and SDMT was also considered to refine the evaluation of disease activity. However, complete data were lacking for several patients. Moreover, when available, these additional clinical parameters did not modify the final X_{status} . Longitudinal clinical information allowing to derive the disease activity status for each subject appears in Table 2. Additional clinical information concerning annual relapse rate and treatment administration appears in [Supplementary material](#).

Permutation tests were employed for inferences (Anderson, 2001). R^2 value was tested against computed statistics after permutation of the data. For a number n of permutations, the X_{status} values were randomly shuffled (constructing a new regressor written X_{status}^π), tested against the unchanged response Y , and generating each time a permuted R^2 value (noted R_π , R_{obs} being the true R^2 value computed without permutation of the data). The condition $X_{status} \neq X_{status}^\pi$ is verified at each permutation. After n permutations (with $n = 5000$ in this study), a p value was computed based on the following formula:

$$p = \frac{\#(R_\pi > R_{obs})}{n + 1},$$

TABLE 2 Longitudinal clinical information and derived disease status score

	EDSS T0	EDSS T1/2	New lesion T1/2	Relapse T1/2	NEDA T1/2	EDSS T1	New lesion T1	Relapse T1	NEDA T1	Time period T0–T1	Score
sub-001	2	2	None	None	YES	2	None	None	YES	30	1
sub-002	1.5	1.5	None	None	YES	1.5	None	None	YES	27	1
sub-003	2	2	None	None	YES	2	None	None	YES	27	1
sub-004	3	3	None	None	YES	3.5	None	None	YES	25	1
sub-005	1	1	None	None	YES	1	None	None	YES	24	1
sub-006	1.5	1.5	None	None	YES	1.5	None	None	YES	24	1
sub-007	2	2	None	None	YES	2	None	None	YES	22	1
sub-008	3.5	4.5	None	N/A	NO	5	None	N/A	NO	51	0
sub-009	2	2.5	None	None	YES	2.5	None	None	YES	57	1
sub-010	6	6	Yes	N/A	NO	6.5	None	None	NO	14	0
sub-011	6	6	None	N/A	YES	6.5	None	N/A	NO	14	1
sub-012	1	1.5	None	None	YES	1.5	None	None	YES	55	1
sub-013	5.5	6	None	N/A	NO	6.5	None	N/A	NO	60	0
sub-014	2.5	3.5	Yes	Yes	NO	3	None	None	YES	57	1
sub-015	4	4.5	None	N/A	NO	5	None	N/A	NO	51	0
sub-016	5	4.5	Yes	N/A	NO	4.5	None	N/A	YES	61	1
sub-017	2	3	Yes	Yes	NO	3	Yes	Yes	NO	56	0

Note: The time period between T0 and T1 is expressed in months.

which estimates the probability of obtaining R_{obs} under the null hypothesis that Y is not correlated to X_{status} . The null hypothesis is rejected if $p < .05$ FDR-corrected for multiple comparisons (Benjamini & Hochberg, 1995), for the 12 tests performed (3 tissue classes with 4 qMRI parameters).

Two-tailed t -tests were applied post hoc on the significant results of permutation tests to compare the AROC distribution between disease status, that is, $X_{status} = 0$ against $X_{status} = 1$. Inferences were conducted at a significance level of .05.

The same pipeline was applied to the brain volumetric changes (BPF, GMF and LF) to test their correlation to the disease activity status.

2.6 | Analysis of lesions and peripheral tissues

For white matter lesions analysis, we did not use AROC but exploited directly the qMRI parameters voxel values. Importantly, with USwL segmentation, the prior lesion mask is only used in a probabilistic way and the estimated posterior lesion map, obtained using MTsat, PD, R1, and FLAIR images, typically showed more extended lesion than clinically visible on the FLAIR image alone. Therefore, we separated focal lesions detected on FLAIR images, with LST segmentation and visual inspection, from their peripheral regions detected on qMRI maps. Two different peripheral regions were considered: one for each time point (T0 and T1). Therefore, at T0, three distinct lesion-related regions were isolated:

- The lesions, as clinically defined, pertaining to hyperintensity on the conventional FLAIR MR image acquired at T0. These are referred to as “focal FLAIR lesion.”
- The peripheral region detected on qMRI maps at T0, at the borders of (but not including) the focal FLAIR lesion. Those are referred to as “initial peripheral lesion.”
- The peripheral region, detected on qMRI maps at follow-up, bordering (but not including) the initial peripheral lesion, further referred to as “later peripheral lesion.” This was computed by masking out the T1 lesion mask with the T0 lesion mask. This region allows us to determine whether its microstructure at T0 forebodes a full-blown plaque, detectable during follow-up. Those sometimes appear hyperintense on FLAIR images.

The three areas were compared between each other and with NAWM, in order to characterize them on a microstructural basis (Figure 2). For an accurate lesion-by-lesion analysis, only enlarging lesions, that is, present in the three masks, were considered for these comparisons.

NAWM region consisted of all white matter voxels, which did not belong to any of the three lesion-related regions. The four areas are not overlapping as no voxel could belong to more than one class at the same time.

For all participants, MTsat, PD, R1, and R2* median values were extracted from each lesion area, considering lesions individually (between 2 and 66 measurements per subject). Similarly, the median

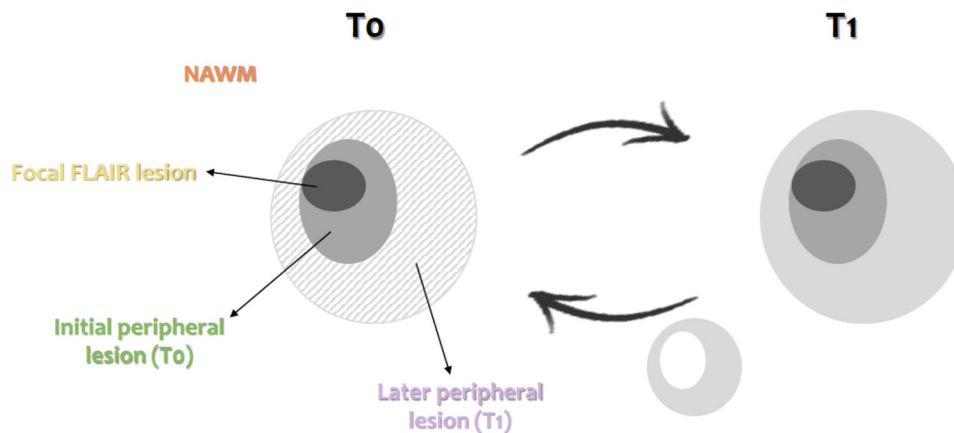


FIGURE 2 Schematic illustration of the NAWM and 3 lesions-related areas: focal FLAIR lesion (dark gray area), initial peripheral lesion detected at T0 (medium gray area), later peripheral lesion detected at T1 (dashed, left, and light gray, right, area).

qMRI values within NAWM were also extracted (one measurement per subject). These values were extracted from T0 and T1 scans separately. Statistical analyses were performed in SAS 9.4 (SAS Institute, Cary, NC). None of the qMRI parameter was normally distributed; therefore, we applied a log transformation on each of them prior to statistical analysis. For each qMRI parameter, a separate Generalized Linear Mixed Model (GLMM) tested the effect of areas (NAWM and the three lesion-related areas), and time points (T0 and T1), as well as their interaction (i.e., area*time), on the median qMRI parameter value, with a first-order autoregressive variance/covariance model and participants as a random factor (intercept). The degrees of freedom were estimated using Kenward–Roger's method. Statistical significance was estimated at $p < .05$ after adjustment for multiple comparison using Tukey's procedure.

3 | RESULTS

3.1 | Volume changes

Brain parenchymal fraction (BPF) annually decreased between T0 and T1 by $-0.67 \pm 1.12\%$ (significantly different from zero; paired-sample t -tests; $t(16) = 2.57$; $p = .0204$) whereas lesion fraction (LF) increased by $22.88 \pm 26.13\%$ ($t(16) = -3.70$; $p = .0019$). GM fraction (GMF) nonsignificantly decreased by $-0.30 \pm 1.44\%$.

3.2 | Analysis of normal appearing tissues

As expected, changes in MTsat and R2* within normal appearing brain tissues (NABT) between T0 and T1 varied across subjects (Figure 3). PD and R1 exhibited similar behaviors, see [Supplementary data](#).

At the group level, with the regression analysis and permutation inference, we observed that the annual rate of change (ARoC) of MTsat and R2* positively regressed with disease status as follows

TABLE 3 Regression coefficients and their associated p values (in parentheses) for the effects of X_{status} on the individual ARoC for each qMRI parameter (MTsat, PD, R1, and R2*) and for volumetric measurements (BPF and LF)

	NAWM	NACGM	NADGM
MTsat	0.039 (.011)*	0.017 (.007)*	0.004 (.749)
PD	-0.018 (.670)	0.405 (.225)	0.250 (.552)
R1	0.009 (.139)	0.004 (.471)	0.010 (.111)
R2*	0.295 (.002)*	0.121 (.092)	0.066 (.770)
BPF	-0.884 (.1562)		
LF	21.23 (.1082)		

*Results significant at $p < .05$, FDR-corrected.

(Table 3): MTsat in NAWM and NACGM and R2* in NAWM significantly increased in patients who fare well ($X_{status} = 1$).

Post hoc t -tests applied on these significant results for a clearer illustration of the difference in disease status (Figure 4) were all significant at a level of .05.

Regarding BPF and LF, their correlation to the disease activity status was not significant (Table 3), suggesting that qMRI parameters are more sensitive to subtle microstructural changes in normal appearing tissues over time than global morphological measurements

3.3 | Analysis of lesion microstructure

The number of enlarging WM lesions between T0 and T1 varied from 2 to 66 across patients, for a total of 741 identified enlarging lesions among all subject, corresponding on average among patients to 63% ($\pm 31\%$) of the amount of initial focal lesions. The number of enlarging lesions did not significantly differ between patients' disease status groups ($t(15) = .244$, $p = .811$).

GLMMs found a significant effect of areas (3 lesion regions and NAWM) for MTsat, R1, R2*, and PD median (MTsat: $F_3 = 35.34$, $p <$

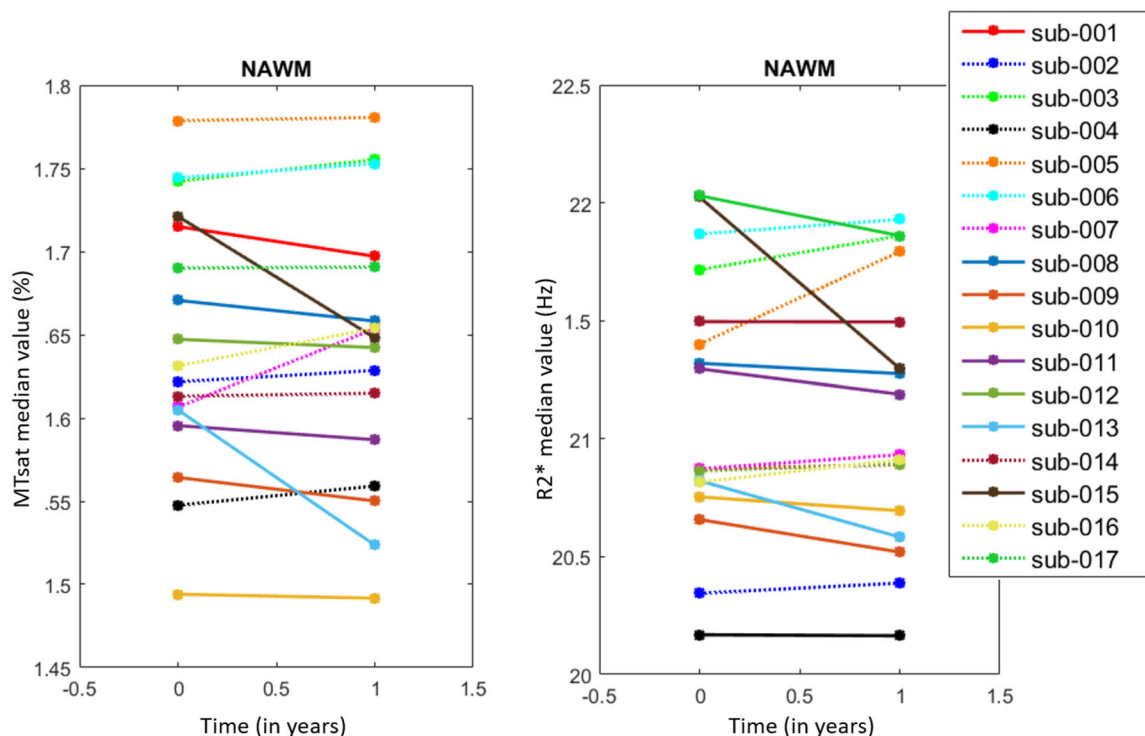


FIGURE 3 Line plots illustrating individual ARoCs for MTsat (left) and R2* (right) in NAWM. Each line corresponds to one subject. Dotted lines represent increasing rates.

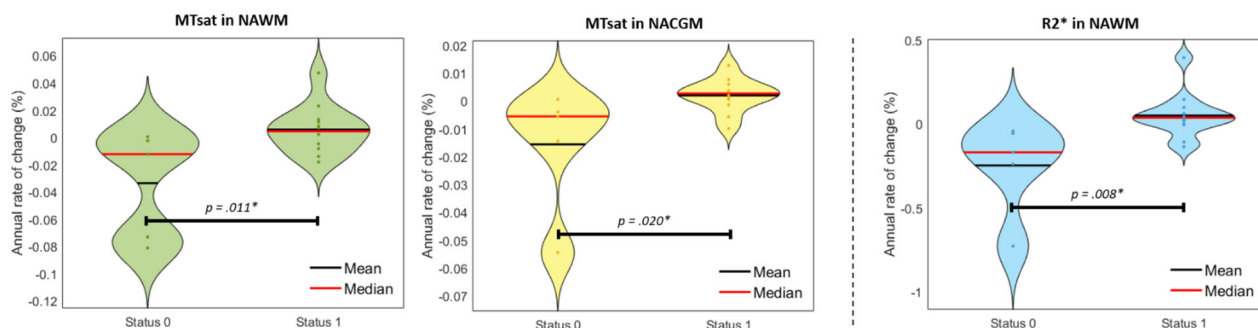


FIGURE 4 Violin plots of significant change rates in microstructure with respect to X_{status} . From left to right: MTsat in NAWM, MTsat in NACGM, R2* in NAWM. * $P < .05$.

.0001, PD: $F_3 = 68.03$, $p < .0001$, R1: $F_3 = 40.26$, $p < .0001$, R2*: $F_3 = 32.32$, $p < .0001$. By contrast, neither time effect (T0 vs. T1; MTsat: $F_3 = 0.36$, $p = .5481$, PD: $F_3 = 1.20$, $p = .2735$, R1: $F_3 = 2.05$, $p = .1520$, R2*: $F_3 = 2.86$, $p = .0911$) nor the area \times time interaction (MTsat: $F_3 = 0.09$, $p = .9671$, PD: $F_3 = 0.14$, $p = .9346$, R1: $F_3 = 0.14$, $p = .9331$, R2*: $F_3 = 0.40$, $p = .7565$) was significant, suggesting the microstructural stability of the initial lesion core. Post hoc tests confirmed significant differences between the four tissue areas.

At times T0 and T1, MTsat, R1, and R2* values were significantly larger in the initial peripheral lesion than FLAIR lesion, in the later peripheral lesion than the initial one, and in the NAWM than later

peripheral lesion. The reverse was observed for PD. The significant difference in parameters between initial and later peripheral lesion at T0 suggests that subtle microstructural changes appear in the periphery of the initial lesion, months before their detection as focal FLAIR lesions at T1. Adjusted p values appear in Figure 5. Detailed statistical results of the GLMMs appear in [Supplementary data](#).

4 | DISCUSSION

This longitudinal study followed up volumetric data and qMRI brain metrics (MTsat, PD, R1, R2*) in 17 patients with multiple sclerosis

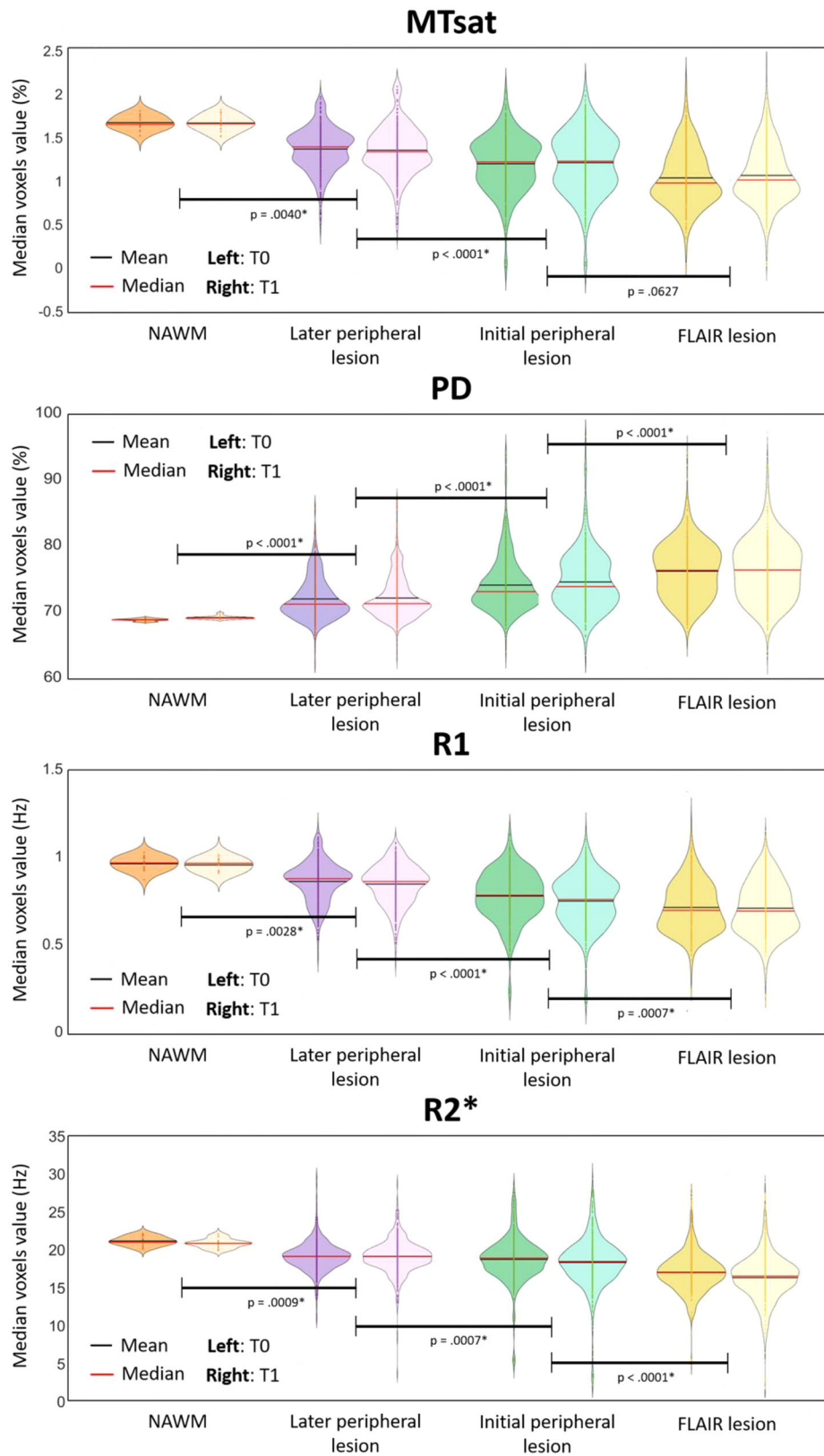


FIGURE 5 Microstructural parameters in NAWM and the 3 lesion-related areas, for each scanning time T0 and T1. p Values were obtained with post hoc tests on the tissue area effect. * $P < .05$.

for a median time interval of 30 months. The main results are threefold. First, the microstructure of normal appearing brain tissues changes over time and these modifications concur with, and potentially drive, clinical evolution. This critical finding suggests that repair mechanism and edema resorption can be monitored *in vivo*. Second, the microstructure within WM plaques is remarkably heterogeneous. Importantly, at their periphery, microstructural alterations foreshadow their expansion, as detected by conventional MRI. Third, as expected, we observed a small but significant brain atrophy and lesion load increase with time.

4.1 | Quantitative MRI parameter time course within NABT

In this study, we used a multiparameter mapping protocol that was gradually optimized and validated for multicentric studies (Leutritz et al., 2020). It provides high-resolution maps of multiple qMRI parameters from data acquired during a single scanning session of acceptable duration. A number of cross-sectional studies using a combination of MT, R1, R2*, or PD parameters reported significant changes in the microstructure of NABT in MS (Andica et al., 2019; Bonnier et al., 2014; Engström et al., 2014; Gracien et al., 2016; Lommers et al., 2019; Lommers et al., 2021; Neema et al., 2007; Reitz et al., 2017; Stevenson et al., 2000). By contrast, longitudinal analyses of multiparameter qMRI data are scarce. A progressive shortening of T2/T2* (Bonnier et al., 2017) or increase in R2* (Elkady et al., 2018; Elkady et al., 2019; Khalil et al., 2015) was reported within the basal ganglia, suggesting increased of myelin and/or iron contents as well as edema resorption. Likewise, PD and T1 increased within a year, suggesting a demyelination and/or axonal loss (Gracien et al., 2017). MTR progressively decreases in NAWM of MS patients over 1 (Laule et al., 2003) or 2 years (Hayton et al., 2012). These abnormalities tend to be more pronounced in progressive phenotypes (Rocca et al., 1999) and were associated to a slow, diffuse, and global myelin pathology.

Here, we showed that MTsat within NAWM and NACGM and R2* values within NAWM increase in clinically stable or improving patients. Because both MTsat and R2* correlate with myelin content (Callaghan et al., 2014; Carey et al., 2018; Hametner et al., 2018; Mangeat et al., 2015; Schmierer et al., 2004; Weiskopf et al., 2015), our results suggest repair mechanisms within NABT of patients who are responding to disease-modifying treatments, despite the initial myelin/axonal loss and independently from WM focal lesion evolution. Such increases could also be explained by an edema/inflammation resorption, but less likely than myelin/axonal density changes since MTsat is the least dependent to water content among the four qMRI parameters. These results echo cross-sectional analyses showing that healthy controls (HC) have higher MTsat and R2* values within the same tissue classes compared to MS patients (Lommers et al., 2019). Annual rates of change of R1 and PD within NABT were not significantly associated with the individual clinical status in this study, although R1 reduction within NABT has already been reported in cross-sectional (Gracien

et al., 2016; Lommers et al., 2019; Neema et al., 2007) and longitudinal (Gracien et al., 2017) studies comparing MS subjects to HC.

4.2 | Lesion microstructure

Focal inflammatory demyelinating lesions have been extensively characterized and are traditionally classified as active, chronic active (smoldering), or inactive plaques according to the presence and distribution of plaque-infiltrating macrophages/microglia (Dutta & Trapp, 2007; Frischer et al., 2015; Lassmann et al., 2001). Focal WM pathology is a constantly evolving process including episodes of demyelination and remyelination but also accumulation of irreversible axonal damage. Age, disease duration, clinical phenotype, as well as disease-modifying treatment all contribute to the dynamic nature of focal WM pathology (Frischer et al., 2015; Lucchinetti et al., 2000). This accounts for the large inter- and intraindividual heterogeneity of MS, which conventional MRI is largely unable to capture. By contrast, quantitative MRI parameters are sensitive to myelin, axonal as well as iron contents and appear as promising markers of plaque dynamics. For instance, MTR was shown to sharply decrease within gadolinium enhancing lesions before recovering during the subsequent months (Dousset et al., 1998; Elskamp et al., 2010; Levesque et al., 2010). Likewise, reduction of MTR within NAWM, days to weeks before the formation of a new active lesion, was also demonstrated (Fazekas et al., 2002; Filippi et al., 1998), and long-term MTR changes in WM plaques were observed in relation with disease progression (Rocca et al., 1999; Zheng et al., 2018). The present study broadens the quantitative characterization of plaque dynamics, in keeping with previous longitudinal studies (Bonnier et al., 2017; Chawla et al., 2018). Two important findings emerge from the results. First, qMRI refines lesion segmentation, as compared to the processing based on the sole FLAIR image. In consequence, the initial lesion revealed by qMRI is typically wider than the plaque detected in FLAIR. Its periphery is characterized by a decrease in MTsat and R2* as compared to NAWM, suggesting an incipient demyelination, reminiscent of the so-called periplaques (Lieury et al., 2014). Moreover, MTsat, R2*, and R1 values progressively decrease from NAWM to plaque core, suggesting a centripetal loss of myelin content. Second, plaque microstructure is altered in plaque periphery before any observable change in conventional MRI signals. This finding suggests, in keeping with neuropathological observations (Frischer et al., 2015; Kuhlmann et al., 2017; Lassmann et al., 2007; Lucchinetti et al., 2000), that sub-clinical ongoing inflammation and/or demyelination takes place in the periphery of an active plaque, well before it is detectable on FLAIR or T1 postgadolinium sequences. If confirmed on larger population samples, this finding might significantly modify treatment management in MS patients.

Another plausible hypothesis explaining the progressive decrease of R2* in initial and later peripheral regions is that iron-containing macrophages could be removing iron from the lesions through perivascular drainage into the extracellular compartment. Previous neuropathological studies have reported an iron loss at the edges of a

subset of MS lesions, depending on their type (active, inactive, smoldering, etc.) as well as the patient's age and disease duration (Hametner et al., 2013; Popescu et al., 2017). Due to the limited sensitivity of $R2^*$ to local iron concentration as compared, for example, to the combined use of $R2^*$ and quantitative susceptibility mapping (QSM) (Hametner et al., 2018), validating this theory would require additional measures, which can better describe iron dynamics in MS lesions and NAWM.

4.3 | Volumetric data

CNS atrophy occurs in all stages of MS, since the preclinical phase of the disease and progresses throughout its course, at a much higher rate than one reported in normal aging (Bermel & Bakshi, 2006; De Stefano et al., 2010; Eshaghi et al., 2018; Zivadinov et al., 2008). In this study, the annual brain percentage volume loss at the group level was 0.67%, which is in line with previous publications (De Stefano et al., 2015). We also showed a significant increase in lesion fraction. Volumetric data (ARoCs) were highly variable across subjects: changes in BPF range from -2.52% to 1.17% and LF from -0.78% to 103.06% . This variability arises from a large number of factors, which do not necessarily relate to MS: age, disease duration, disease phenotype, disease-modifying treatment, circadian rhythm, hydration, etc. (Bermel & Bakshi, 2006; Zivadinov et al., 2008).

Moreover, annual changes in brain parenchymal fraction as well as lesion fraction only partially correlated to patients' disease status, in accordance with a large amount of publications (Enzinger et al., 2015; Gracien et al., 2017). This highlights the lack of specificity and sensitivity of volumetric measurements, at least at the individual level.

It can appear odd that brain atrophy progresses in parallel to repair mechanisms, as suggested by qMRI parameters. However, BPF reduction is minimal and is not significant (see Table 3) between T0 and T1. One should keep in mind that cortical atrophy is an irreversible phenomenon. Given the inter- and intraindividual heterogeneity of MS progression, it is possible that patients who have undergone neuron-axonal loss at some point in the disease might be able to remyelinate their remaining axons, hopefully through therapeutic intervention or lifestyle changes. Besides, axonal remyelination is not always effective. Here we showed that variations in MTsat and $R2^*$ correlated to the disease activity status, but our clinical evaluation based on EDSS is undoubtedly imprecise. Once again, the size and heterogeneity of our cohort limits the interpretation of such results.

4.4 | Study limitation

As mentioned here above, the small size and heterogeneous aspect of the present dataset constitute major limitations of this study. Indeed, it is composed of only 17 patients, with a rather broad range of characteristics such as age, disease duration, disease phenotype, disease-modifying treatment, etc., which are known to influence the disability state of the patient and thus their ability to put together repair mechanisms within cerebral tissues (Bodini et al., 2016; Frischer

et al., 2015; Lassmann, 2013; Lassmann et al., 2001; Lucchinetti et al., 2000; Patrikios et al., 2006). In addition, the time interval between two scanning sessions varied rather widely across patients (between 14 and 61 months), although it was brought back to an annual rate where possible. All of these parameters were imposed by standard clinical follow-up. Therefore, these results should not be over-interpreted but are nevertheless promising and call for a replication with a larger and more homogeneous or controlled set of MS patients. Larger longitudinal studies are currently being held and will probably confirm these preliminary results.

A second limitation is the absence of longitudinal MRI data acquired in a control group of healthy subjects. However, we considered that literature of longitudinal studies of healthy subjects that analyzed tissue microstructure could constitute a solution for comparison with MS patients. For example, in Bonnier et al. (2017), the control group did not show any significant differences regarding T1, T2*, or MTR measurements over 2 years, and the median age of their group is quite similar to ours (34.3 vs. 36 years). Also, in Elkady et al. (2018), they found no longitudinal $R2^*$ effect in their control groups, even with an age range superior to ours. Moreover, the median age of our population (<60 years), as well as the short period between two scanning sessions (median of 14 months), suggests that microstructural alterations would not be noticeable in a healthy participants group, as many quantitative aging studies detected differences over much larger time periods (Callaghan et al., 2014; Draganski et al., 2011; Gracien et al., 2017).

5 | CONCLUSION

These preliminary results highlight the relevance of multiple qMRI data in the monitoring of MS disease, highlighting subtle changes within NABT and plaque dynamics in relation with repair or disease progression. Of course, large-scale longitudinal study would be needed to reproduce these findings and better exploit the full potential of qMRI parameters.

ACKNOWLEDGMENTS

The authors are particularly thankful for the patients who took part in this study.

FUNDING

N.V., E.L., and C.P. are supported by the Fonds de la Recherche Scientifique (F.R.S-FNRS Belgium).

DATA AVAILABILITY STATEMENT

The data that support the findings of this study are available on request from the corresponding author. The data are not publicly available due to privacy or ethical restrictions.

ORCID

Nora Vandeleene  <https://orcid.org/0000-0003-0619-788X>

Emilie Lommers  <https://orcid.org/0000-0001-7965-4629>

Christophe Phillips  <https://orcid.org/0000-0002-4990-425X>

PEER REVIEW

The peer review history for this article is available at <https://publons.com/publon/10.1002/brb3.2923>.

REFERENCES

- Andersen, S. M., Rapcsak, S. Z., & Beeson, P. M. (2010). Cost function masking during normalization of brains with focal lesions: Still a necessity? *Neuroimage*, 53(1), 78–84. <https://doi.org/10.1016/j.neuroimage.2010.06.003>
- Anderson, M. J. (2001). Permutation tests for univariate or multivariate analysis of variance and regression. *Canadian Journal of Fisheries and Aquatic Sciences*, 58(3), 626–639. <https://doi.org/10.1139/f01-004>
- Andica, C., Hagiwara, A., Kamagata, K., Yokoyama, K., Shimoji, K., Saito, A., Takenaka, Y., Nakazawa, M., Hori, M., Cohen-Adad, J., Takemura, M. Y., Hattori, N., & Aoki, S. (2019). Gray matter alterations in early and late relapsing-remitting multiple sclerosis evaluated with synthetic quantitative magnetic resonance imaging. *Scientific Reports*, 9(1), 8147. <https://doi.org/10.1038/s41598-019-44615-3>
- Ashburner, J., & Ridgway, G. R. (2013). Symmetric diffeomorphic modeling of longitudinal structural MRI. *Frontiers in Neuroscience*, 6. <https://doi.org/10.3389/fnins.2012.00197>
- Ashburner, J., & Friston, K. J. (2005). Unified segmentation. *Neuroimage*, 26(3), 839–851. <https://doi.org/10.1016/j.neuroimage.2005.02.018>
- Bagnato, F., Hametner, S., Boyd, E., Endmayr, V., Shi, Y., Ikonomidou, V., Chen, G., Pawate, S., Lassmann, H., Smith, S., & Welch, E. B. (2018). Untangling the R2* contrast in multiple sclerosis: A combined MRI-Histology study at 7.0 tesla. *PLoS ONE*, 13(3), e0193839. <https://doi.org/10.1371/journal.pone.0193839>
- Benjamini, Y., & Hochberg, Y. (1995). Controlling the false discovery rate: A practical and powerful approach to multiple testing. *Journal of the Royal Statistical Society. Series B (Methodological)*, 57(1), 289–300.
- Bermel, R. A., & Bakshi, R. (2006). The measurement and clinical relevance of brain atrophy in multiple sclerosis. *The Lancet Neurology*, 5(2), 158–170. [https://doi.org/10.1016/S1474-4422\(06\)70349-0](https://doi.org/10.1016/S1474-4422(06)70349-0)
- Bodini, B., Veronese, M., García-Lorenzo, D., Battaglini, M., Poirion, E., Chardain, A., Freeman, L., Louapre, C., Tchikviladze, M., Papeix, C., Dollé, F., Zalc, B., Lubetzki, C., Bottlaender, M., Turkheimer, F., & Stankoff, B. (2016). Dynamic imaging of individual remyelination profiles in multiple sclerosis. *Annals of Neurology*, 79(5), 726–738. <https://doi.org/10.1002/ana.24620>
- Bonnier, G., Maréchal, B., Fartaria, M. J., Falkowskiy, P., Marques, J. P., Simioni, S., Schlupe, M., Pasquier, R. D. u., Thiran, J. -P., Krueger, G., & Granziera, C. (2017). The combined quantification and interpretation of multiple quantitative magnetic resonance imaging metrics enlightens longitudinal changes compatible with brain repair in relapsing-remitting multiple sclerosis patients. *Frontiers in Neurology*, 8, 506. <https://doi.org/10.3389/fneur.2017.00506>
- Bonnier, G., Roche, A., Romascano, D., Simioni, S., Meskaldji, D., Rotzinger, D., Lin, Y. -C., Menegaz, G., Schlupe, M., Pasquier, R. D. u., Sumpf, T. J., Frahm, J., Thiran, J. -P., Krueger, G., & Granziera, C. (2014). Advanced MRI unravels the nature of tissue alterations in early multiple sclerosis. *Annals of Clinical and Translational Neurology*, 1(6), 423–432. <https://doi.org/10.1002/acn3.68>
- Brown, R. A., Narayanan, S., & Arnold, D. L. (2014). Imaging of repeated episodes of demyelination and remyelination in multiple sclerosis. *Neuroimage: Clinical*, 6, 20–25. <https://doi.org/10.1016/j.nicl.2014.06.009>
- Callaghan, M. F., Freund, P., Draganski, B., Anderson, E., Cappelletti, M., Chowdhury, R., Diedrichsen, J., FitzGerald, T. H. B., Smittenaar, P., Helms, G., Lutti, A., & Weiskopf, N. (2014). Widespread age-related differences in the human brain microstructure revealed by quantitative magnetic resonance imaging. *Neurobiology of Aging*, 35(8), 1862–1872. <https://doi.org/10.1016/j.neurobiolaging.2014.02.008>
- Callaghan, M. F., Helms, G., Lutti, A., Mohammadi, S., & Weiskopf, N. (2015). A general linear relaxometry model of r_1 using imaging data: General linear relaxometry model of r_1 . *Magnetic Resonance in Medicine*, 73(3), 1309–1314. <https://doi.org/10.1002/mrm.25210>
- Carey, D., Caprini, F., Allen, M., Lutti, A., Weiskopf, N., Rees, G., Callaghan, M. F., & Dick, F. (2018). Quantitative MRI provides markers of intra-, inter-regional, and age-related differences in young adult cortical microstructure. *Neuroimage*, 182, 429–440. <https://doi.org/10.1016/j.neuroimage.2017.11.066>
- Chawla, S., Kister, I., Sinnecker, T., Wuerfel, J., Brisset, J. -C., Paul, F., & Ge, Y. (2018). Longitudinal study of multiple sclerosis lesions using ultra-high field (7T) multiparametric MR imaging. *PLoS ONE*, 13(9), e0202918. <https://doi.org/10.1371/journal.pone.0202918>
- Depierreux, F., Parmentier, E., Mackels, L., Baquero, K., Degueldre, C., Baiteau, E., Salmon, E., Phillips, C., Bahri, M. A., Maquet, P., & Garraux, G. (2021). Parkinson's disease multimodal imaging: F-DOPA PET, neuromelanin-sensitive and quantitative iron-sensitive MRI. *Npj Parkinson's Disease*, 7(1), 57. <https://doi.org/10.1038/s41531-021-00199-2>
- De Stefano, N., Giorgio, A., Battaglini, M., Rovaris, M., Sormani, M. P., Barkhof, F., Korteweg, T., Enzinger, C., Fazekas, F., Calabrese, M., Dinacci, D., Tedeschi, G., Gass, A., Montalban, X., Rovira, A., Thompson, A., Comi, G., Miller, D. H., & Filippi, M. (2010). Assessing brain atrophy rates in a large population of untreated multiple sclerosis subtypes. *Neurology*, 74(23), 1868–1876. <https://doi.org/10.1212/WNL.0b013e3181e24136>
- De Stefano, N., Stromillo, M. L., Giorgio, A., Bartolozzi, M. L., Battaglini, M., Baldini, M., Portaccio, E., Amato, M. P., & Sormani, M. P. (2015). Establishing pathological cut-offs of brain atrophy rates in multiple sclerosis. *Journal of Neurology, Neurosurgery & Psychiatry*, 87(1), 93–99. <https://doi.org/10.1136/jnnp-2014-309903>
- Dousset, V., Gayou, A., Brochet, B., & Caille, J. -M. (1998). Early structural changes in acute MS lesions assessed by serial magnetization transfer studies. *Neurology*, 51(4), 1150–1155. <https://doi.org/10.1212/WNL.51.4.1150>
- Draganski, B., Ashburner, J., Hutton, C., Kherif, F., Frackowiak, R. S. J., Helms, G., & Weiskopf, N. (2011). Regional specificity of MRI contrast parameter changes in normal ageing revealed by voxel-based quantification (VBQ). *Neuroimage*, 55(4), 1423–1434. <https://doi.org/10.1016/j.neuroimage.2011.01.052>
- Dutta, R., & Trapp, B. D. (2007). Pathogenesis of axonal and neuronal damage in multiple sclerosis. *Neurology*, 68(22), S22–S31. <https://doi.org/10.1212/01.wnl.0000275229.13012.32>
- Edwards, L. J., Kirilina, E., Mohammadi, S., & Weiskopf, N. (2018). Microstructural imaging of human neocortex in vivo. *Neuroimage*, 182, 184–206. <https://doi.org/10.1016/j.neuroimage.2018.02.055>
- Elkady, A. M., Cobzas, D., Sun, H., Blevins, G., & Wilman, A. H. (2018). Discriminative analysis of regional evolution of iron and myelin/calcium in deep gray matter of multiple sclerosis and healthy subjects: Analysis of iron and myelin in mS. *Journal of Magnetic Resonance Imaging*, 48(3), 652–668. <https://doi.org/10.1002/jmri.26004>
- Elkady, A. M., Cobzas, D., Sun, H., Seres, P., Blevins, G., & Wilman, A. H. (2019). Five year iron changes in relapsing-remitting multiple sclerosis deep gray matter compared to healthy controls. *Multiple Sclerosis and Related Disorders*, 33, 107–115. <https://doi.org/10.1016/j.msard.2019.05.028>
- Elskamp, I. j., Knol, D. I., Vrenken, H., Karas, G., Meijerman, A., Filippi, M., Kappos, L., Wagner, K., Pohl, C., Sandbrink, R., Polman, C. H., Uitdehaag, B. M. J., & Barkhof, F. (2010). Lesional magnetization transfer ratio: A feasible outcome for remyelinating treatment trials in multiple sclerosis. *Multiple Sclerosis Journal*, 16(6), 660–669. <https://doi.org/10.1177/1352458510364630>
- Engström, M., Warntjes, J. B. M., Tisell, A., Landtblom, A. -M., & Lundberg, P. (2014). Multi-parametric representation of voxel-based quantitative magnetic resonance imaging. *PLoS ONE*, 9(11), e111688. <https://doi.org/10.1371/journal.pone.0111688>
- Enzinger, C., Barkhof, F., Ciccarelli, O., Filippi, M., Kappos, L., Rocca, M. A., Rovira, A., Schneider, T., de Stefano, N., Vrenken, H.,

- Wheeler-Kingshott, C., Wuerfel, J., & Fazekas, F. (2015). Nonconventional MRI and microstructural cerebral changes in multiple sclerosis. *Nature Reviews Neurology*, 11(12), 676–686. <https://doi.org/10.1038/nrneuro.2015.194>
- Eshaghi, A., Prados, F., Brownlee, W. J., Altmann, D. R., Tur, C., Cardoso, M. J., De Angelis, F., van de Pavert, S. H., Cawley, N., De Stefano, N., Stromillo, M. L., Battaglini, M., Ruggieri, S., Gasperini, C., Filippi, M., Rocca, M. A., Rovira, A., Sastre-Garriga, J., Vrenken, H., ... Ciccarelli, O. (2018). Deep gray matter volume loss drives disability worsening in multiple sclerosis: Deep gray matter volume loss. *Annals of Neurology*, 83(2), 210–222. <https://doi.org/10.1002/ana.25145>
- Fazekas, F., Ropele, S., Enzinger, C., Seifert, T., & Strasser-Fuchs, S. (2002). Quantitative magnetization transfer imaging of pre-lesional white-matter changes in multiple sclerosis. *Multiple Sclerosis Journal*, 8(6), 479–484. <https://doi.org/10.1191/1352458502ms8600a>
- Filippi, M., Rocca, M. A., Horsfield, M. A., Hametner, S., Geurts, J. J., Comi, G., & Lassmann, H. (2013). Imaging cortical damage and dysfunction in multiple sclerosis. *JAMA Neurology*, 70(5), 556–564. <https://doi.org/10.1001/jamaneuro.2013.1954>
- Filippi, M., Rocca, M. A., Martino, G., Horsfield, M. A., & Comi, G. (1998). Magnetization transfer changes in the normal appearing white matter precede the appearance of enhancing lesions in patients with multiple sclerosis. *Annals of Neurology*, 43(6), 809–814. <https://doi.org/10.1002/ana.410430616>
- Frischer, J. M., Bramow, S., Dal-Bianco, A., Lucchinetti, C. F., Rauschka, H., Schmidbauer, M., Laursen, H., Sorensen, P. S., & Lassmann, H. (2009). The relation between inflammation and neurodegeneration in multiple sclerosis brains. *Brain*, 132(5), 1175–1189. <https://doi.org/10.1093/brain/awp070>
- Frischer, J. M., Weigand, S. D., Guo, Y., Kale, N., Parisi, J. E., Pirko, I., Mandrekar, J., Bramow, S., Metz, I., Brück, W., Lassmann, H., & Lucchinetti, C. F. (2015). Clinical and pathological insights into the dynamic nature of the white matter multiple sclerosis plaque: Dynamic nature of MS plaque. *Annals of Neurology*, 78(5), 710–721. <https://doi.org/10.1002/ana.24497>
- Gracien, R. -M., Jurcoane, A., Wagner, M., Reitz, S. C., Mayer, C., Volz, S., Hof, S. -M., Fleischer, V., Droby, A., Steinmetz, H., Groppa, S., Hattingen, E., Deichmann, R., & Klein, J. C. (2016). Multimodal quantitative MRI assessment of cortical damage in relapsing-remitting multiple sclerosis: Cortical quantitative MRI in RRMS. *Journal of Magnetic Resonance Imaging*, 44(6), 1600–1607. <https://doi.org/10.1002/jmri.25297>
- Gracien, R. -M., Reitz, S. C., Hof, S. -M., Fleischer, V., Droby, A., Wahl, M., Steinmetz, H., Groppa, S., Deichmann, R., & Klein, J. C. (2017). Longitudinal quantitative MRI assessment of cortical damage in multiple sclerosis: A pilot study: Longitudinal cortical QMRI in mS. *Journal of Magnetic Resonance Imaging*, 46(5), 1485–1490. <https://doi.org/10.1002/jmri.25685>
- Gracien, R. M., Nürnberger, L., Hok, P., Hof, S. -M., Reitz, S. C., Rüb, U., Steinmetz, H., Hilker-Roggendorf, R., Klein, J. C., Deichmann, R., & Baudrexel, S. (2017). Evaluation of brain ageing: A quantitative longitudinal MRI study over 7 years. *European Radiology*, 27, 1568–1576. <https://doi.org/10.1007/s00330-016-4485-1>
- Granziera, C., Wuerfel, J., Barkhof, F., Calabrese, M., De Stefano, N., Enzinger, C., Evangelou, N., Granziera, C., Wuerfel, J., Barkhof, F., Calabrese, M., De Stefano, N., Enzinger, C., Evangelou, N., Filippi, M., Geurts, J. J. G., Reich, D. S., Rocca, M. A., Ropele, S., ... Kappos, L. (2021). Quantitative magnetic resonance imaging towards clinical application in multiple sclerosis. *Brain*, 144(5), 1296–1311. <https://doi.org/10.1093/brain/awab029>
- Guillemain, C., Lommers, E., Delrue, G., Gester, E., Maquet, P., & Collette, F. (2022). The complex interplay between trait fatigue and cognition in multiple sclerosis. *Psychologica Belgica*, 62(1), 108. <https://doi.org/10.5334/pb.1125>
- Haider, L., Zrzavy, T., Hametner, S., Höftberger, R., Bagnato, F., Grabner, G., Tractnig, S., Pfeifenbring, S., Brück, W., & Lassmann, H. (2016). The topography of demyelination and neurodegeneration in the multiple sclerosis brain. *Brain*, 139(3), 807–815. <https://doi.org/10.1093/brain/awv398>
- Hametner, S., Endmayr, V., Deistung, A., Palmrich, P., Prihoda, M., Haimburger, E., Menard, C., Feng, X., Haider, T., Leisser, M., Köck, U., Kaider, A., Höftberger, R., Robinson, S., Reichenbach, J. R., Lassmann, H., Traxler, H., Tractnig, S., & Grabner, G. (2018). The influence of brain iron and myelin on magnetic susceptibility and effective transverse relaxation—A biochemical and histological validation study. *Neuroimage*, 179, 117–133. <https://doi.org/10.1016/j.neuroimage.2018.06.007>
- Hametner, S., Wimmer, I., Haider, L., Pfeifenbring, S., Brück, W., & Lassmann, H. (2013). Iron and neurodegeneration in the multiple sclerosis brain. *Annals of Neurology*, 74(6), 848–861. <https://doi.org/10.1002/ana.23974>
- Hayton, T., Furby, J., Smith, K. J., Altmann, D. R., Brenner, R., Chataway, J., Hunter, K., Tozer, D. J., Miller, D. H., & Kapoor, R. (2012). Longitudinal changes in magnetisation transfer ratio in secondary progressive multiple sclerosis: Data from a randomised placebo controlled trial of lamotrigine. *Journal of Neurology*, 259(3), 505–514. <https://doi.org/10.1007/s00415-011-6212-9>
- Helms, G., Dathe, H., & Dechent, P. (2010). Modeling the influence of TR and excitation flip angle on the magnetization transfer ratio (MTR) in human brain obtained from 3D spoiled gradient echo MRI. *Magnetic Resonance in Medicine*, 64(1), 177–185. <https://doi.org/10.1002/mrm.22379>
- Hulst, H. E., & Geurts, J. J. G. (2011). Gray matter imaging in multiple sclerosis: What have we learned? *BMC Neurology*, 11(1), 153. <https://doi.org/10.1186/1471-2377-11-153>
- Khalil, M., Langkammer, C., Pichler, A., Pinter, D., Gatteringer, T., Bachmaier, G., Ropele, S., Fuchs, S., Enzinger, C., & Fazekas, F. (2015). Dynamics of brain iron levels in multiple sclerosis: A longitudinal 3T MRI study. *Neurology*, 84(24), 2396–2402. <https://doi.org/10.1212/WNL.0000000000001679>
- Klein, J. C., Rolinski, M., Griffanti, L., Szeewczyk-Krolikowski, K., Baig, F., Ruffmann, C., Groves, A. R., Menke, R. A. L., Hu, M. T., & Mackay, C. (2018). Cortical structural involvement and cognitive dysfunction in early Parkinson's disease. *NMR in Biomedicine*, 31(4), e3900. <https://doi.org/10.1002/nbm.3900>
- Kolb, H., Absinta, M., Beck, E. S., Ha, S. -K., Song, Y., Norato, G., Cortese, I., Sati, P., Nair, G., & Reich, D. S. (2021). 7T MRI differentiates remyelinated from demyelinated multiple sclerosis lesions. *Annals of Neurology*, 90(4), 612–626. <https://doi.org/10.1002/ana.26194>
- Kuhlmann, T., Ludwin, S., Prat, A., Antel, J., Brück, W., & Lassmann, H. (2017). An updated histological classification system for multiple sclerosis lesions. *Acta Neuropathologica*, 133(1), 13–24. <https://doi.org/10.1007/s00401-016-1653-y>
- Kutzelnigg, A., Lucchinetti, C. F., Stadelmann, C., Brück, W., Rauschka, H., Bergmann, M., Schmidbauer, M., Parisi, J. E., & Lassmann, H. (2005). Cortical demyelination and diffuse white matter injury in multiple sclerosis. *Brain*, 128(11), 2705–2712. <https://doi.org/10.1093/brain/awh641>
- Lassmann, H. (2013). Pathology and disease mechanisms in different stages of multiple sclerosis. *Journal of the Neurological Sciences*, 333(1–2), 1–4. <https://doi.org/10.1016/j.jns.2013.05.010>
- Lassmann, H., Brück, W., & Lucchinetti, C. (2001). Heterogeneity of multiple sclerosis pathogenesis: Implications for diagnosis and therapy. *Trends in Molecular Medicine*, 7(3), 115–121. [https://doi.org/10.1016/S1471-4914\(00\)01909-2](https://doi.org/10.1016/S1471-4914(00)01909-2)
- Lassmann, H., Brück, W., & Lucchinetti, C. F. (2007). The immunopathology of multiple sclerosis: An overview. *Brain Pathology*, 17(2), 210–218. <https://doi.org/10.1111/j.1750-3639.2007.00064.x>
- Laule, C., Vavasour, I. M., Whittall, K. P., Oger, J., Paty, D. W., Li, D. K. B., MacKay, A. L., & Arnold, D. L. (2003). Evolution of focal and diffuse magnetisation transfer abnormalities in multiple sclerosis. *Journal of Neurology*, 250(8), 924–931. <https://doi.org/10.1007/s00415-003-1115-z>
- Lema, A., Bishop, C., Malik, O., Mattoscio, M., Ali, R., Nicholas, R., Muraro, P. A., Matthews, P. M., Waldman, A. D., & Newbould, R. D. (2017). A

- comparison of magnetization transfer methods to assess brain and cervical cord microstructure in multiple sclerosis: MT of brain and c-spine in mS. *Journal of Neuroimaging*, 27(2), 221–226. <https://doi.org/10.1111/jon.12377>
- Leutritz, T., Seif, M., Helms, G., Samson, R. S., Curt, A., Freund, P., & Weiskopf, N. (2020). Multiparameter mapping of relaxation (R1, R2 *), proton density and magnetization transfer saturation at 3 T: A multicenter dual-vendor reproducibility and repeatability study. *Human Brain Mapping*, 41(15), 4232–4247. <https://doi.org/10.1002/hbm.25122>
- Levesque, I. R., Giacomini, P. S., Narayanan, S., Ribeiro, L. T., Sled, J. G., Arnold, D. L., & Bruce Pike, G. (2010). Quantitative magnetization transfer and myelin water imaging of the evolution of acute multiple sclerosis lesions: Quantitative MT and t_2 in Acute MS lesions. *Magnetic Resonance in Medicine*, 63(3), 633–640. <https://doi.org/10.1002/mrm.22244>
- Lieury, A., Chanal, M., Androdias, G., Reynolds, R., Cavagna, S., Giraudon, P., Confavreux, C., & Nataf, S. (2014). Tissue remodeling in periplaque regions of multiple sclerosis spinal cord lesions: Glia remodeling in MS spinal cord. *Glia*, 62(10), 1645–1658. <https://doi.org/10.1002/glia.22705>
- Lommers, E., Guillemin, C., Reuter, G., Fouarge, E., Delrue, G., Collette, F., Degueldre, C., Balteau, E., Maquet, P., & Phillips, C. (2021). VOXEL-BASED quantitative MRI reveals spatial patterns of grey matter alteration in multiple sclerosis. *Human Brain Mapping*, 42(4), 1003–1012. <https://doi.org/10.1002/hbm.25274>
- Lommers, E., Simon, J., Reuter, G., Delrue, G., Dive, D., Degueldre, C., Balteau, E., Phillips, C., & Maquet, P. (2019). Multiparameter MRI quantification of microstructural tissue alterations in multiple sclerosis. *NeuroImage: Clinical*, 23, 101879. <https://doi.org/10.1016/j.nicl.2019.101879>
- Lorio, S., Fresard, S., Adaszewski, S., Kherif, F., Chowdhury, R., Frackowiak, R. S., Ashburner, J., Helms, G., Weiskopf, N., Lutti, A., & Draganski, B. (2016). New tissue priors for improved automated classification of subcortical brain structures on MRI. *NeuroImage*, 130, 157–166. <https://doi.org/10.1016/j.neuroimage.2016.01.062>
- Lucchinetti, C., Brück, W., Parisi, J., Scheithauer, B., Rodriguez, M., & Lassmann, H. (2000). Heterogeneity of multiple sclerosis lesions: Implications for the pathogenesis of demyelination. *Annals of Neurology*, 47(6), 707–717. [https://doi.org/10.1002/1531-8249\(200006\)47:6<707::AID-ANA3330.CO;2-Q](https://doi.org/10.1002/1531-8249(200006)47:6<707::AID-ANA3330.CO;2-Q)
- Lutti, A., Hutton, C., Finsterbusch, J., Helms, G., & Weiskopf, N. (2010). Optimization and validation of methods for mapping of the radiofrequency transmit field at 3T: Optimized RF transmit field mapping at 3T. *Magnetic Resonance in Medicine*, 64(1), 229–238. <https://doi.org/10.1002/mrm.22421>
- Lutti, A., Stadler, J., Josephs, O., Windischberger, C., Speck, O., Bernarding, J., Hutton, C., & Weiskopf, N. (2012). Robust and fast whole brain mapping of the RF transmit field B1 at 7T. *PLoS ONE*, 7(3), e32379. <https://doi.org/10.1371/journal.pone.0032379>
- Mangeat, G., Govindarajan, S. T., Mainero, C., & Cohen-Adad, J. (2015). Multivariate combination of magnetization transfer, t_2^* and B0 orientation to study the myelo-architecture of the in vivo human cortex. *NeuroImage*, 119, 89–102. <https://doi.org/10.1016/j.neuroimage.2015.06.033>
- Moon, N., Bullitt, E., Leemput, K., & Gerig, G. (2002). Automatic brain and tumor segmentation. In *Medical image computing and computer-assisted intervention—MICCAI 2002*. T. Dohi & R. Kikinis (Eds.), Lecture Notes in Computer Science (Vol. 2488, pp. 372–379). Berlin, Heidelberg: Springer Berlin Heidelberg. https://doi.org/10.1007/3-540-45786-0_46
- Mottershead, J. P., Schmierer, K., Clemence, M., Thornton, J. S., Scaravilli, F., Barker, G. J., Tofts, P. S., Newcombe, J., Cuzner, M. L., Ordidge, R. J., McDonald, W. I., & Miller, D. H. (2003). High field MRI correlates of myelin content and axonal density in multiple sclerosis. *Journal of Neurology*, 250(11), 1293–1301. <https://doi.org/10.1007/s00415-003-0192-3>
- Neema, M., Stankiewicz, J., Arora, A., Dandamudi, V. S. R., Batt, C. E., Guss, Z. D., Al-Sabbagh, A., & Bakshi, R. (2007). T1- and T2-based MRI measures of diffuse gray matter and white matter damage in patients with multiple sclerosis. *Journal of Neuroimaging*, 17, 165–215. <https://doi.org/10.1111/j.1552-6569.2007.00131.x>
- Nürnberg, L., Gracien, R. -M., Hok, P., Hof, S. -M., Rüb, U., Steinmetz, H., Hilker, R., Klein, J. C., Deichmann, R., & Baudrexel, S. (2017). Longitudinal changes of cortical microstructure in Parkinson's disease assessed with T1 relaxometry. *NeuroImage: Clinical*, 13, 405–414. <https://doi.org/10.1016/j.nicl.2016.12.025>
- Pandit, L. (2019). No evidence of disease activity (NEDA) in multiple sclerosis—Shifting the goal posts. *Annals of Indian Academy of Neurology*, 22(3), 261. https://doi.org/10.4103/aian.AIAN_159_19
- Patrikios, P., Stadelmann, C., Kutzelnigg, A., Rauschka, H., Schmidbauer, M., Laursen, H., Sorensen, P. S., Bruck, W., Lucchinetti, C., & Lassmann, H. (2006). Remyelination is extensive in a subset of multiple sclerosis patients. *Brain*, 129(12), 3165–3172. <https://doi.org/10.1093/brain/awl217>
- Polman, C. H., Reingold, S. C., Banwell, B., Clanet, M., Cohen, J. A., Filippi, M., Fujihara, K., Havrdova, E., Hutchinson, M., Kappos, L., Lublin, F. D., Montalban, X., O'Connor, P., Sandberg-Wollheim, M., Thompson, A. J., Waubant, E., Weinstenker, B., & Wolinsky, J. S. (2011). Diagnostic criteria for multiple sclerosis: 2010 revisions to the McDonald criteria. *Annals of Neurology*, 69(2), 292–302. <https://doi.org/10.1002/ana.22366>
- Popescu, B. F., Frischer, J. M., Webb, S. M., Tham, M., Adiele, R. C., Robinson, C. A., Fitz-Gibbon, P. D., Weigand, S. D., Metz, I., Nehzati, S., George, G. N., Pickering, I. J., Brück, W., Hametner, S., Lassmann, H., Parisi, J. E., Yong, G., & Lucchinetti, C. F. (2017). Pathogenic implications of distinct patterns of iron and zinc in chronic MS lesions. *Acta Neuropathologica*, 134(1), 45–64. <https://doi.org/10.1007/s00401-017-1696-8>
- Popescu, G. h., Bogdan, F., & Lucchinetti, C. F. (2012). Meningeal and cortical grey matter pathology in multiple sclerosis. *BMC Neurology*, 12(1), 11. <https://doi.org/10.1186/1471-2377-12-11>
- Preibisch, C., & Deichmann, R. (2009). Influence of RF spoiling on the stability and accuracy of t_1 mapping based on spoiled FLASH with varying flip angles: Influence of RF spoiling on t_1 mapping. *Magnetic Resonance in Medicine*, 61(1), 125–135. <https://doi.org/10.1002/mrm.21776>
- Reitz, S. C., Hof, S. -M., Fleischer, V., Brodski, A., Gröger, A., Gracien, R. -M., Droby, A., Steinmetz, H., Ziemann, U., Zipp, F., Deichmann, R., & Klein, J. C. (2017). Multi-parametric quantitative MRI of normal appearing white matter in multiple sclerosis, and the effect of disease activity on t_2 . *Brain Imaging and Behavior*, 11(3), 744–753. <https://doi.org/10.1007/s11682-016-9550-5>
- Reuter, G., Lommers, E., Balteau, E., Simon, J., Phillips, C., Scholtes, F., Martin, D., Lombard, A., & Maquet, P. (2020). Multiparameter quantitative histological MRI values in high-grade gliomas: A potential biomarker of tumor progression. *Neuro-Oncology Practice*, 7(6), 646–655. <https://doi.org/10.1093/nop/npaa047>
- Rocca, M. A., Mastrorlando, G., Rodegher, M., Comi, G., & Filippi, M. (1999). Long-term changes of magnetization transfer-derived measures from patients with relapsing-remitting and secondary progressive multiple sclerosis. *Ajnr American Journal of Neuroradiology*, 20, 21–827.
- Schmidt, P., Gaser, C., Arsic, M., Buck, D., Förschler, A., Berthele, A., Hoshi, M., Ilg, R., Schmid, V. J., Zimmer, C., Hemmer, B., & Mühlau, M. (2012). An automated tool for detection of FLAIR-hyperintense white-matter lesions in multiple sclerosis. *NeuroImage*, 59(4), 3774–3783. <https://doi.org/10.1016/j.neuroimage.2011.11.032>
- Schmierer, K., Scaravilli, F., Altmann, D. R., Barker, G. J., & Miller, D. H. (2004). Magnetization transfer ratio and myelin in postmortem multiple sclerosis brain. *Annals of Neurology*, 56(3), 407–415. <https://doi.org/10.1002/ana.20202>
- Stankiewicz, J. M., Neema, M., & Ceccarelli, A. (2014). Iron and multiple sclerosis. *Neurobiology of Aging*, 35, S5158. <https://doi.org/10.1016/j.neurobiolaging.2014.03.039>
- Stevenson, V. L., Parker, G. J. M., Barker, G. J., Birnie, K., Tofts, P. S., Miller, D. H., & Thompson, A. J. (2000). Variations in T1 and T2 relaxation times

- of normal appearing white matter and lesions in multiple sclerosis. *Journal of the Neurological Sciences*, 178(2), 81–87. [https://doi.org/10.1016/S0022-510X\(00\)00339-7](https://doi.org/10.1016/S0022-510X(00)00339-7)
- Stüber, C., Morawski, M., Schäfer, A., Labadie, C., Wähnert, M., Leuze, C., Streicher, M., Barapatre, N., Reimann, K., Geyer, S., Spemann, D., & Turner, R. (2014). Myelin and iron concentration in the human brain: A quantitative study of MRI contrast. *Neuroimage*, 93, 95–106. <https://doi.org/10.1016/j.neuroimage.2014.02.026>
- Tabelow, K., Balteau, E., Ashburner, J., Callaghan, M. F., Draganski, B., Helms, G., Kherif, F., Leutritz, T., Lutti, A., Phillips, C., Reimer, E., Ruthotto, L., Seif, M., Weiskopf, N., Ziegler, G., & Mohammadi, S. (2019). HMRI—A toolbox for quantitative MRI in neuroscience and clinical research. *Neuroimage*, 194, 191–210. <https://doi.org/10.1016/j.neuroimage.2019.01.029>
- Thompson, A. J., Banwell, B. L., Barkhof, F., Carroll, W. M., Coetzee, T., Comi, G., Correale, J., Fazekas, F., Filippi, M., Freedman, M. S., Fujihara, K., Galetta, S. L., Hartung, H. P., Kappos, L., Lublin, F. D., Marrie, R. A., Miller, A. E., Miller, D. H., & Montalban, X. (2018). Diagnosis of multiple sclerosis: 2017 revisions of the McDonald criteria. *The Lancet Neurology*, 17(2), 162–173. [https://doi.org/10.1016/S1474-4422\(17\)30470-2](https://doi.org/10.1016/S1474-4422(17)30470-2)
- Trapp, B. D., Peterson, J., Ransohoff, R. M., Rudick, R., Mörk, S., & Bö, L. (1998). Axonal transection in the lesions of multiple sclerosis. *New England Journal of Medicine*, 338(5), 278–285. <https://doi.org/10.1056/NEJM199801293380502>
- Van Waesberghe, J. H. T. M., Kamphorst, W., De Groot, C. J. A., Van Walderveen, M. A. A., Castelijns, J. A., Ravid, R., Lycklama a Nijeholt, G. J., van der Valk, P., Polman, C. H., Thompson, A. J., & Barkhof, F. (1999). Axonal loss in multiple sclerosis lesions: Magnetic resonance imaging insights into substrates of disability. *Annals of Neurology*, 46(5), 747–754. [https://doi.org/10.1002/1531-8249\(199911\)46:5\(747::AID-ANA10\)3.0.CO;2-4](https://doi.org/10.1002/1531-8249(199911)46:5(747::AID-ANA10)3.0.CO;2-4)
- Wang, C. T., Barnett, M., & Barnett, Y. (2019). Imaging the multiple sclerosis lesion: Insights into pathogenesis, progression and repair. *Current Opinion in Neurology*, 32(3), 338–345. <https://doi.org/10.1097/WCO.0000000000000698>
- Weiskopf, N., Callaghan, M. F., Josephs, O., Lutti, A., & Mohammadi, S. (2014). Estimating the apparent transverse relaxation time ($R2^*$) from images with different contrasts (ESTATICS) reduces motion artifacts. *Frontiers in Neuroscience*, 8, <https://doi.org/10.3389/fnins.2014.00278>
- Weiskopf, N., Mohammadi, S., Lutti, A., & Callaghan, M. F. (2015). Advances in MRI-Based computational neuroanatomy: From morphometry to in-Vivo histology. *Current Opinion in Neurology*, 28(4), 313–322. <https://doi.org/10.1097/WCO.0000000000000222>
- Zheng, Y., Lee, J. -C., Rudick, R., & Fisher, E. (2018). Long-term magnetization transfer ratio evolution in multiple sclerosis white matter lesions: Long-term MTR evolution in MS WM lesions. *Journal of Neuroimaging*, 28(2), 191–198. <https://doi.org/10.1111/jon.12480>
- Zivadinov, R., Reder, A. T., Filippi, M., Minagar, A., Stuve, O., Lassmann, H., Racke, M. K., Dwyer, M. G., Frohman, E. M., & Khan, O. (2008). Mechanisms of action of disease-modifying agents and brain volume changes in multiple sclerosis. *Neurology*, 71(2), 136–144. <https://doi.org/10.1212/01.wnl.0000316810.01120.05>

SUPPORTING INFORMATION

Additional supporting information can be found online in the Supporting Information section at the end of this article.

How to cite this article: Vandeleene, N., Guillemin, C., Dauby, S., Requier, F., Charonitis, M., Chylinski, D., Balteau, E., Maquet, P., Lommers, E., & Phillips, C. (2023). Using quantitative magnetic resonance imaging to track cerebral alterations in multiple sclerosis brain: A longitudinal study. *Brain and Behavior*, 13, e2923. <https://doi.org/10.1002/brb3.2923>